Results in Physics 75 (2025) 108338

Contents lists available at ScienceDirect

Results in Physics

journal homepage: www.elsevier.com/locate/rinp

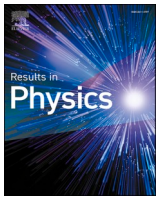

High-performance all-optical photonic crystal synapse based on Mach-Zehnder interferometer and directional coupler utilizing GSST phase-change material

Amir Hossein Abdollahi Nohoji, Parviz Keshavarzi, Mohammad Danaie *

Faculty of Electrical and Computer Engineering, Semnan University, Semnan, Iran

ARTICLE INFO

Keywords:
Neural network synapse
Photonic crystal
Cavity
Mach-Zehnder Interferometer
Phase change material
Photonic neuromorphic

ABSTRACT

This paper presents a novel architecture for all-optical photonic crystals, leveraging the integration of Mach-Zehnder interferometers and directional couplers for advanced optical neuromorphic synapses. By utilizing photonic crystals and germanium-antimony-selenium-tellurium (GSST) phase-change materials, we achieve precise control over optical transmission. The use of photonic crystals enables a compact footprint and significantly reduces the device size compared to conventional silicon photonics, offering a key advantage in achieving higher integration density for optical neuromorphic systems. Comprehensive finite-difference time-domain (FDTD) simulations demonstrate that incorporating a photonic crystal cavity at the input port significantly enhances single-mode operation, leading to an output signal transmission of more than 99 %. Furthermore, variations in the crystallinity fraction of phase-change material (PCM) rods significantly influence the output signal transmission, enabling precise control of the signal dynamics. Under amorphous and fully crystalline conditions of the GSST-PCM rods, the signal transmission rate varies between −0.02 dB and −13.5 dB, highlighting the profound impact of phase-state changes on system performance. This innovative photonic crystal platform offers a promising avenue for the realization of next-generation optical synapses, paving the way for advanced optical neural networks and machine learning.

Introduction

Recently, optical information-processing systems and neuromorphic neural networks have attracted increasing interest. These advancements not only facilitate the high-speed and high-precision processing of optical data but also pave the way for novel paradigms in implementing machine learning algorithms and information processing at micro- and nano-scales [1–4]. Within this landscape, neuromorphic synapses play a pivotal role in optical neural networks, and their design, aimed at emulating the synaptic characteristics of the human brain, has the potential to revolutionize the fields of optical signal processing and machine learning [5–10]. These synapses, analogous to the neural synapses in the human brain, can execute complex computations with exceptional speed and accuracy, thereby enhancing the efficiency of artificial intelligence systems and deep learning algorithms [11,12].

Photonic crystals, as optical structures with the capable of manipulating and guiding light at the nanoscale, have garnered significant attention, particularly in the realms of optical signal processing, logic gates, modulation, and information storage [13–18]. Owing to their inherent ability to control light propagation and engender unique characteristics, such as sharp variations in light transmission and dispersion, these structures have attracted researchers, especially in signal processing and information storage. The inherent precision of photonic crystals in light manipulation and signal modulation makes them highly promising for the development of next-generation optical processing systems and neuromorphic synapses [19,20].

The integration of phase-change materials (PCMs) [21–24] with photonic crystals offers a broad spectrum of possibilities for phase-state tuning and precise optical signal control [25–27]. Specifically, these materials can dynamically regulate the transmission and scattering of optical signals across different spectral ranges by transitioning between their amorphous and crystalline states [28–30]. This property makes them highly advantageous for the development of neuromorphic synapses, which require precise signal regulation and adaptive dynamic behavior.

In this paper, we present a novel architecture for all-optical photonic

* Corresponding author.
E-mail address: danaie@semnan.ac.ir (M. Danaie).

https://doi.org/10.1016/j.rinp.2025.108338
Received 30 March 2025; Received in revised form 2 June 2025; Accepted 18 June 2025
Available online 19 June 2025

crystal neuromorphic synapses based on the synergistic integration of Mach-Zehnder interferometer (MZI) [31–33], cavity [34–36], and directional coupler [37,38] devices. The utilization of this combination, particularly in conjunction with silicon rod-type photonic crystals and phase-change materials, such as GSST [39–41], enables precise control over signal transmission and enhances the performance of optical processing systems.

In the proposed structure, input signals are applied to the optical synapse as optical wavelengths, and their weighting is achieved through the crystallization rate of PCM rods positioned along the optical path. The weighted signals are combined in a summation block and then compared against a threshold value within a nonlinear activation function block, such as sigmoid or ReLU, which plays a crucial role in enabling complex and nonlinear behaviors of neural networks [42–44]. When the sum of the inputs exceeds this threshold, the neuron generates an output signal (Fig. 1).

The output signal is evaluated in the error block, where, using learning algorithms such as backpropagation and the delta rule [45,46], the crystallization rate of the PCM is controlled by adjusting the energy and duration of the input optical pulses. This process enables precise modulation of synaptic weights and simulates the learning mechanism in optical neural networks.

These algorithms operate based on the principle of error minimization. During this process, the neuron's output is compared to a target value, and corrective signals are generated according to the calculated error to adjust the synaptic weights. Gradually, the output error decreases and network training improves, allowing the network to generalize effectively to new inputs.

The stages of this algorithm are briefly summarized in the training and weight adjustment flowchart of the artificial neural network (Fig. 2), which illustrates the interactions between system components and the error reduction process.

In this study, the focus is placed on the design and optimization of the optical synapse structure, with the control of the PCM crystallization rate considered as the key mechanism for weight modulation.

The proposed structure is designed specifically for high-precision optical signal processing and transmission with minimal interference, which significantly reduces the device footprint compared with prior silicon photonic implementations. Furthermore, numerical simulations utilizing both the FDTD and finite element method (FEM) techniques have substantiated the effectiveness of this architecture in achieving optimal transmission and improved efficiency in single-mode optical systems.

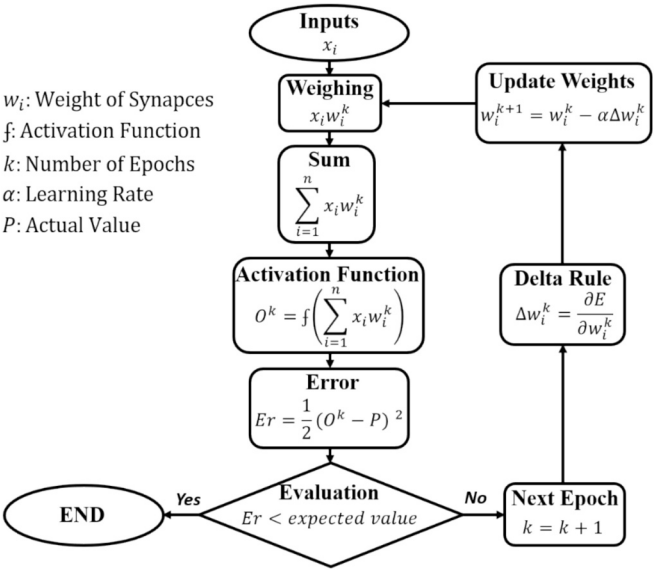

Fig. 2. Flowchart of the training and weight adjustment algorithm in an artificial neural network.

This study aims to develop an advanced and innovative all-optical neuromorphic synapse based on photonic crystals that can be utilized as a powerful tool for optical information processing and the realization of optical neural networks in all-optical machine learning systems.

Proposed Mach-Zehnder interferometer structure

The proposed structure presents a novel optical architecture that synergistically integrates Mach-Zehnder interferometers with directional couplers. This innovative combination enables the realization of advanced and optimized optical structures. The MZI structure is implemented by incorporating two parallel directional couplers, as shown in Fig. 3.

The proposed structure comprises a triangular lattice photonic crystal formed from silicon rods with a lattice constant of a = 0.506 μm. The silicon rods had a radius of ra = 0.2a and a refractive index of n = 3.5, and were positioned on a SiO_2 substrate with a refractive index of 1.44.

In this structure, we incorporated a photonic crystal cavity in the

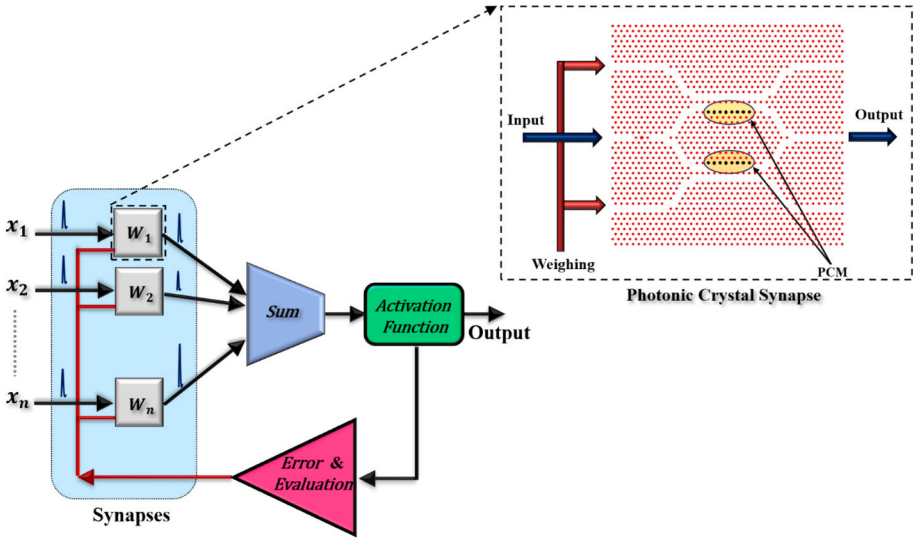

Fig. 1. Schematic of an artificial neuron with all-optical, tunable photonic crystal synapses.

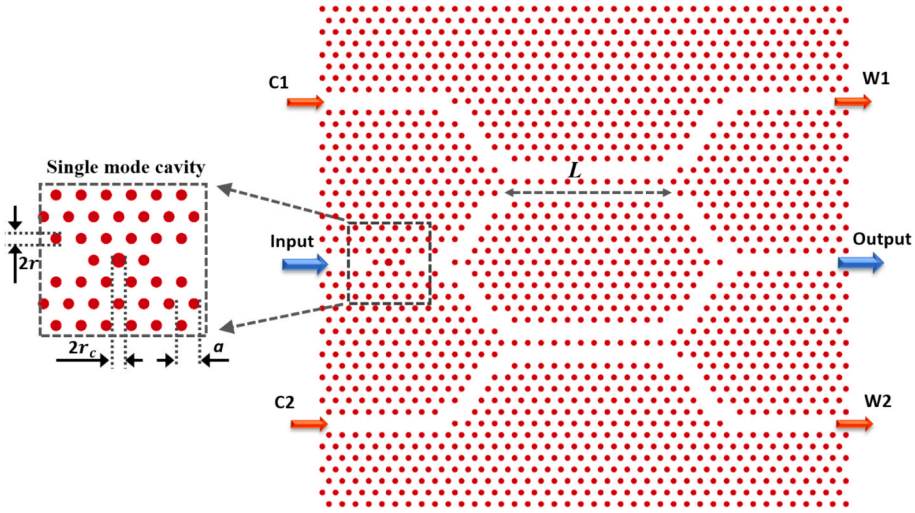

Fig. 3. Schematic of the proposed photonic crystal structure.

input waveguide path, with a central rod radius of rc = 0.275a. This cavity is specifically designed to enforce tunable single-mode operation of the optical signals at the input, thereby enhancing the precision and efficiency of the system in optical information processing.

By applying coherent optical signals to input paths C1 and C2, the signals were independently routed to outputs W1 and W2, respectively.

The dispersion diagram for the supercell of the MZI structure is presented using the plane wave expansion (PWE) method, as shown in Fig. 4. The results of this analysis reveal that two distinct eigenmodes with different characteristics are formed in the structure: even (symmetric) and odd (antisymmetric). As mentioned in previous studies [47,48], light propagating in one waveguide of directional coupler can periodically couple to other waveguide after traveling a specific distance (coupling length).

The required coupling length (L_c) for complete coupling between waveguides is derived from the relationship between the propagation constants of the two modes, as given in Eq. (1). Based on this relationship, a relatively short coupling length of approximately $L_c = 5.5a$ was obtained at a normalized frequency of 0.384. Therefore, to ensure the reflection effect and increase the efficiency of the Mach-Zehnder interferometer, a length $L = 11a$ (approximately twice the coupling length) was selected.

$$L_c = \frac{\pi}{k_{even} - k_{odd}} \tag{1}$$

where K_{even} and K_{odd} represent propagation constants for even and odd modes, respectively.

Numerical simulations based on the FDTD method demonstrated that applying a signal to the input port resulted in over 99 % signal transmission at the output at a wavelength of λ = 1320 nm, as illustrated in Fig. 5a. This high transmission efficiency underscores the superior capability of the proposed structure to direct and transfer optical signals via the MZI configuration. The presence of a cavity at the input port ensured single-mode operation. In this regard, crosstalk in the W1 and W2 channels remains negligible, measured at less than −18 dB. This significant reduction in crosstalk highlights the precise separation of the transmitted optical signals, ensuring independent signal reception at the output, with maximum transmission and minimal interference.

Fig. 5b illustrates the signal transmission through W1 when in-phase signals are applied at inputs C1 and C2. The results indicate that more than 99 % of the signal at a wavelength of λ = 1467 nm is reflected into the primary waveguide via the directional couplers, with only a negligible portion coupling into the MZI output.

In addition, the electric-field profile presented in Fig. 6a distinctly highlights the operation of the MZI structure within this design, confirming that the proposed configuration efficiently channels the optical mode along the input and output ports. Integrating an MZI with a cavity in its input path not only preserves and tunes the transmitted signal along the desired path but also ensures single-mode signal reception at the output. Fig. 6b illustrates the signal propagation and electric field distribution within the structure, clearly demonstrating the field coupling in the directional couplers for guiding signals from inputs C1 and C2.

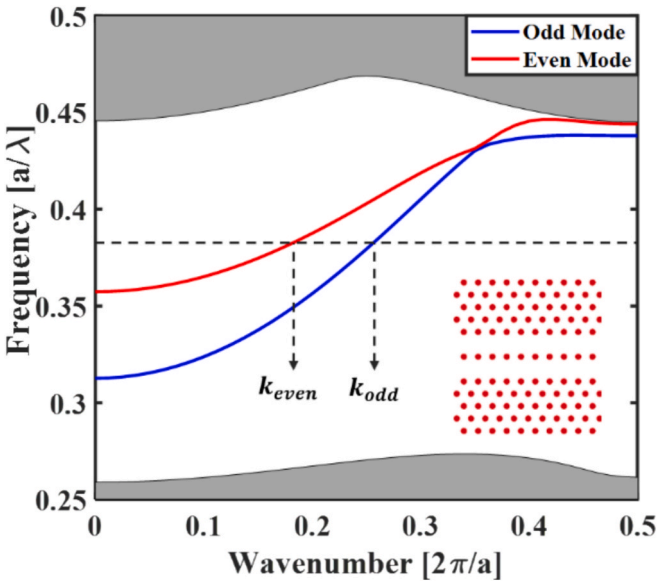

Fig. 4. The dispersion diagram for the photonic crystal super-cell structure.

$Ge_2Sb_2Se_4Te_1$ phase change material

Phase-change materials are essential for advancing data storage technologies, optical modulation, and optical neuromorphic synapses, owing to their reversible switching between amorphous and crystalline phases. $Ge_2Sb_2Se_4Te_1$ (GSST) is a promising advanced PCM, which has recently attracted considerable interest in photonics. This material has been introduced as an efficient alternative to $Ge_2Sb_2Te_5$ (GST), offering notable advantages, such as lower optical losses, high refractive index contrast, and broad transparency over a wide wavelength range.

Moreover, its broad transparency window, extending beyond 16 μm,

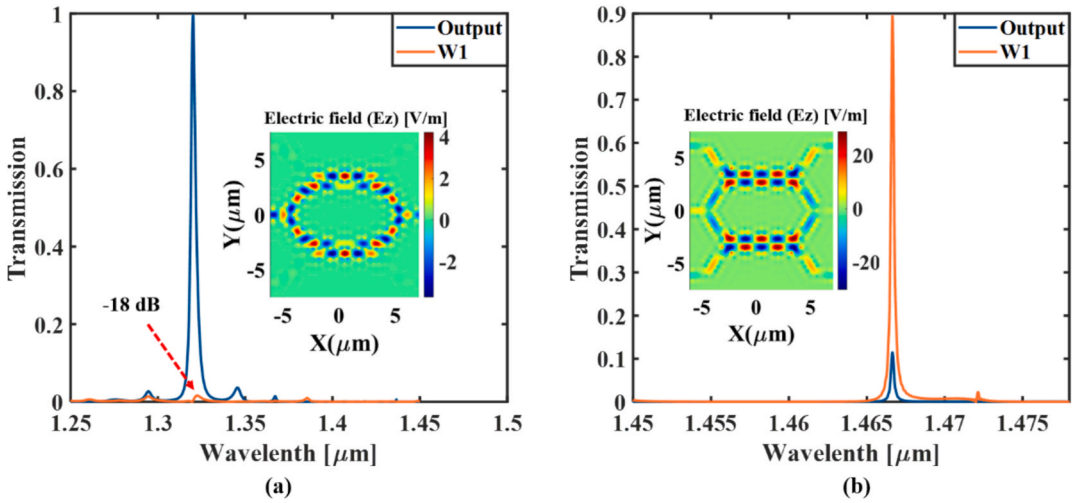

Fig. 5. Transmission characteristics and z-component of the electric field (E_z), (a) Signal launched from the input port, (b) Signal launched from C1 and C2 inputs.

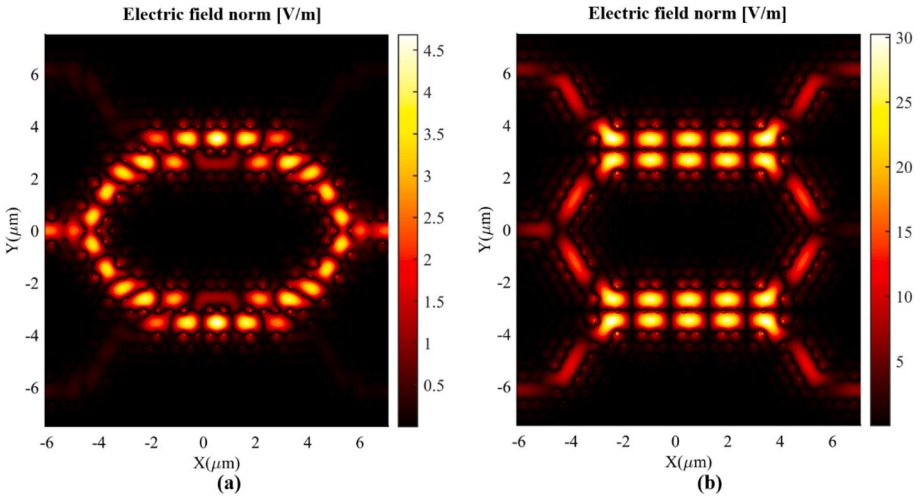

Fig. 6. Normalized electric field profile (a) Signal launched from the input port, (b) Signal launched from C1 and C2 inputs.

makes it well suited for photonic applications such as modulators, optical switching, and neuromorphic computing [39]. Another key advantage of GSST-PCM is its amorphous-state dielectric properties, which result in reduced optical losses and better refractive index matching with silicon at telecommunication wavelengths, thereby facilitating seamless integration with silicon photonics technology.

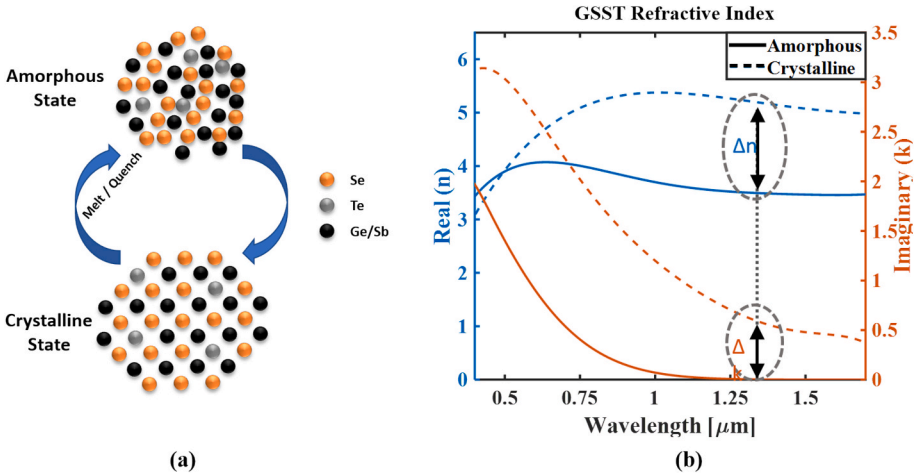

Fig. 7. (a) Phase transition of GSST-PCM between amorphous and crystalline states. (b) Wavelength-dependent refractive index of GSST-PCM in amorphous and crystalline states.

Owing to these superior characteristics, GSST-PCM is recognized as an efficient platform for dynamically tunable and non-volatile photonic circuits, addressing the key limitations of traditional PCM-based optical systems. With these advantages, GSST-PCMs have emerged as a powerful alternative to conventional PCMs, playing a pivotal role in developing controllable photonic circuits with optimized performance and minimal losses.

Fig. 7a illustrates the phase transition between the crystalline and amorphous states in GSST materials, which exhibit either an ordered crystalline or a disordered amorphous configuration. To induce a crystalline phase in the GSST material from an amorphous state, the temperature of GSST-PCM must be maintained between the crystallization temperature ($T_c \approx 523$ °K) and melting temperature ($T_m \approx 900$ °K) [39,49–51], which is achieved by applying optical pulses [6,52,53]. Fig. 7b illustrates the refractive indices of GSST-PCM in both the fully amorphous and crystalline states across different wavelengths [54–56]. These refractive index changes substantially influence the optical response of the systems, particularly the light interaction dynamics with phase-change materials such as GSST.

The multi-level partially crystallized states of GSST-PCM have been utilized in various applications, including multi-level memory devices and photonic neural networks. These multi-level crystallized states are typically triggered using normal-incident laser pulses, confirming their presence through Raman spectroscopy. To achieve an accurate multi-level crystallized state, it is crucial to select the appropriate peak intensity and duration of the control pulses. The crystallization fraction (η) of GST-PCM affects both the real and imaginary components of its refractive index, as described by the Lorentz-Lorenz relationship in Eqs. (2)-(3) [52,57,58]. Changes in the crystallization fraction lead to significant modifications in the optical properties of the material, particularly in its refractive index. These variations are essential in optical and data storage applications because shifts in the refractive index can profoundly impact the optical behavior and performance of devices that rely on these materials.

$$\frac{\varepsilon_{eff}(\eta)-1}{\varepsilon_{eff}(\eta)+2}=\eta\frac{\varepsilon_c-1}{\varepsilon_c+2}+(1-\eta)\frac{\varepsilon_a-1}{\varepsilon_a+2} \tag{2}$$

$$\sqrt{\varepsilon_{eff}(\eta)}=n+ik \tag{3}$$

where ε_c and ε_a denote the crystallization and amorphous wavelength-dependent permittivity of the GSST-PCM, respectively.

Proposed MZI synapse equipped with GSST-PCM

Considering the overlap of the electric fields during signal propagation from the input and through paths C1 and C2, the output transmission can be actively controlled by embedding GSST-PCM rods within the MZI arms. In this structure, 16 rods composed of GSST-PCM are placed within the MZI arms, as illustrated in Fig. 8. These phase-change materials enable precise adjustment of the crystallinity fraction (η) and facilitate efficient modulation of signal transmission at the MZI output.

The phase changes in the PCM rods induced by the state transition of the GSST material can effectively regulate the transmission and scattering of optical signals along the MZI arms. This capability enables precise control over the signal propagation and processing within the structure. This capability enables the precise modulation of signal propagation and processing within the structure, offering tunability for optical systems, particularly all-optical neural synapses. Consequently, this method has significant potential for applications in optical information processing and advanced neural networks.

In optical neural synapses, the transmission of input signals can be modulated by applying optical signals through weighting paths [6]. Similarly, in the proposed structure, the crystallinity fraction of the GSST-PCM rods can be adjusted using signals with specific powers and durations through inputs C1 and C2 [6]. These variations in the crystallinity fraction significantly affected the optical properties of the structure, enabling dynamic control over the transmission behavior within the MZI pathway.

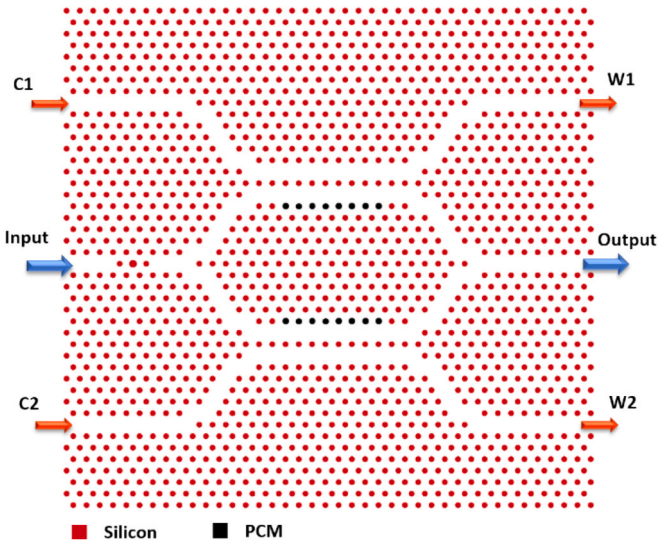

Fig. 8. Proposed MZI synapse equipped with GSST-PCM structure.

The transmission of the fully amorphous and crystalline states of the GSST-PCM rods in the MZI output path is shown in Fig. 9a. The results indicate that in the amorphous state, the transmission was −0.02 dB. In contrast, for the fully crystalline state, it decreased to −13.5 dB. These changes, mainly owing to variations in the crystallinity fraction of the GSST-PCM rods, have a notable impact on the intensity of the transmitted wavelength. The transmission levels for various crystallinity fractions are shown in Fig. 9b. By applying weighting signals through inputs C1 and C2, the crystallinity fraction of the GSST-PCM rods can be adjusted.

Results and discussion

In the MZI-based structure, to ensure uniform and stable phase modulation in the GSST rods located in the interferometer arms, the input optical signals to these two arms are maintained in-phase. By altering the phase state of the GSST rods (amorphous or crystalline) in each arm, the transmitted light intensity along the corresponding path changes accordingly. Fig. 10 and Table 1 present the simulation results for the four possible combinations of GSST phase states in the C1 and C2 paths. These results demonstrate that the GSST rods in each arm exhibit high sensitivity to phase-state changes, enabling independent control of the GSST rods' crystallinity level in each path.

Therefore, this analysis demonstrates that the phase state of the GSST-PCM rods in each path can be directly controlled by the intensity and duration of the optical excitation applied via the C1 and C2 arms. Accordingly, by precisely tuning the excitation parameters, it is possible to regulate the crystallinity rate in the GSST rods, thereby enabling effective control over the absorption and transmission of light in the output path.

To evaluate the stability and practical feasibility of the proposed photonic synapse structure, a comprehensive tolerance analysis of key parameters is performed. This analysis examines the impact of potential fabrication-induced variations in geometric and optical parameters, including the radius of GSST rods, the lattice constant, and the refractive index of silicon.

Considering common fabrication processes such as lithography and material deposition, natural fluctuations in dimensions and material properties occur, which are particularly critical in submicron photonic structures. Accordingly, simulations incorporate variation ranges of ±5

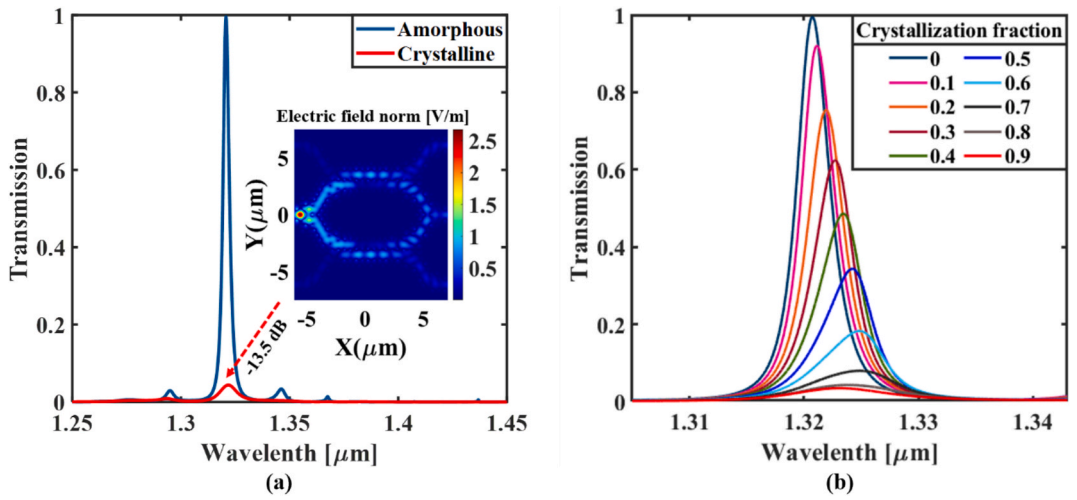

Fig. 9. Transmission characteristics of proposed synapse structure for: (a) Fully amorphous and crystalline states, (b) Various crystallinity fractions.

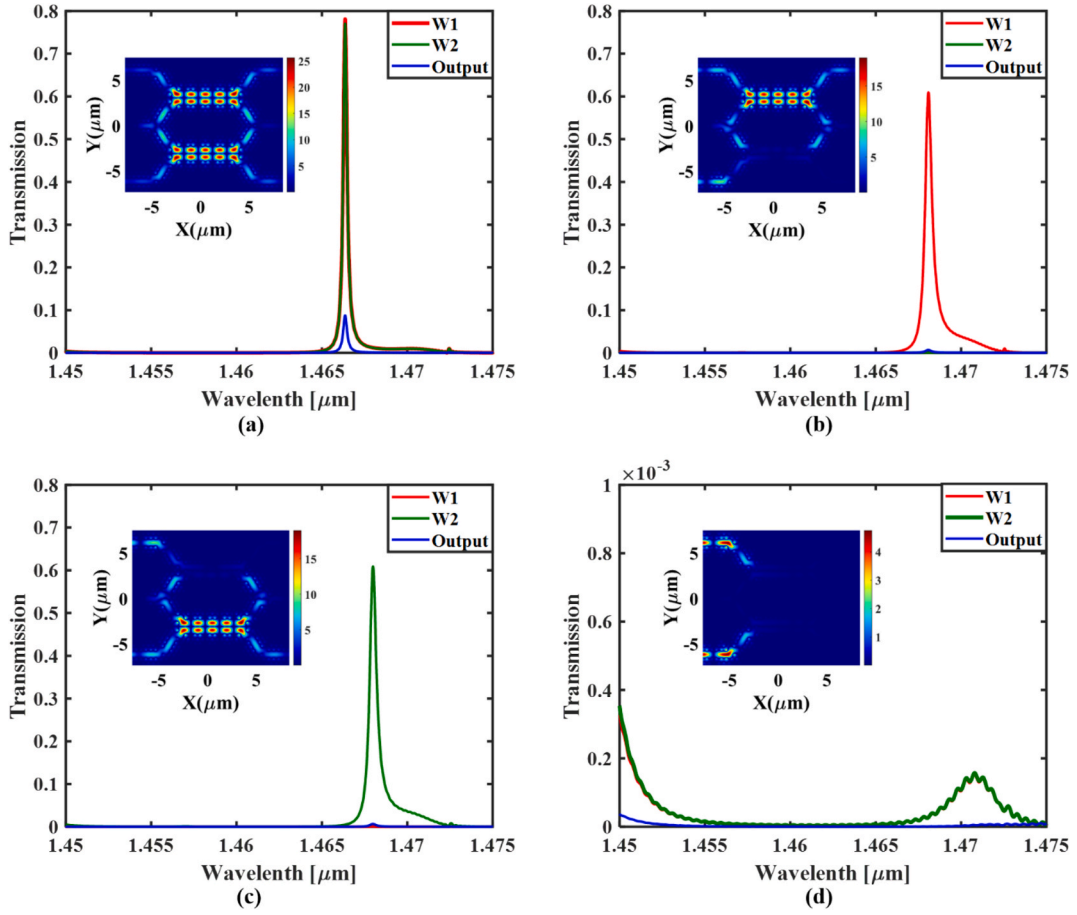

Fig. 10. Transmission spectra and electric field profiles for the four possible phase-state combinations of GSST-PCM rods in C1 and C2 arms: (a) both in the amorphous state, (b) C1 amorphous and C2 crystalline, (c) C1 crystalline and C2 amorphous, and (d) both in the crystalline state.

% for rod radius and lattice constant, and ±0.01 for the silicon refractive index, representing a realistic span consistent with typical fabrication tolerances.

Fig. 11 illustrate the effects of these fluctuations on key performance metrics such as transmission efficiency, resonance wavelength position, and insertion loss. The results indicate that:

- Variations in the GSST-PCM rod radius induce minor shifts in resonance wavelength, while the core functionality remains intact.
- Changes in lattice constant affect the photonic bandgap position and resonance behavior, causing resonance wavelength shifts without degrading performance.
- Fluctuations in silicon refractive index lead to slight resonance wavelength changes; however, the quality factor (Q-factor) and

Table 1
Transmission for the four GSST-PCM rod phase-state combinations in the MZI arms.

C1	C2	W1	W2	Output
Am	Am	0.78	0.78	0.088
Am	Cry	0.61	0.0001	0.007
Cry	Am	0.0001	0.61	0.007
Cry	Cry	0.0002	0.0002	0

synaptic behavior remain stable within the specified variation ranges.

These findings confirm that the proposed design is robust against fabrication-induced variations and maintains its fundamental performance under small structural changes. This robustness ensures the reliability and practical applicability of the structure for implementation in real photonic neuromorphic systems.

Numerical simulations in this study are performed using the FDTD method. To prevent non-physical reflections at the simulation boundaries, perfectly matched layer (PML) boundary conditions are applied. A uniform grid size of 10 nm is chosen to ensure sufficient accuracy in modeling electromagnetic field variations and the resonant behavior of the structure.

To guarantee result convergence, the total field energy decay is monitored until it reduces below 10^{-5} of its initial value. Additionally, a mesh size sensitivity analysis is conducted to evaluate the adequacy of the selected grid resolution. As illustrated in Fig. 12, the resonance wavelength position is examined as functions of the mesh size. The results clearly demonstrate that the 10 nm grid provides sufficient accuracy and more decrease in mesh size does not significantly affect the simulation outcomes.

Furthermore, to conduct a more precise evaluation of the structure's performance under realistic conditions, complementary numerical analyses based on the FEM have been carried out. The results from these analyses exhibit good agreement with those obtained from FDTD simulations, thereby confirming the accuracy of the designed model.

Additionally, to assess the device performance in three-dimensional configurations and to investigate the feasibility of vertical optical confinement, 3D-FDTD simulations are performed for the proposed structure. In this setup, two metallic layers are considered as reflective boundaries at the top and bottom of the structure, and the height of the silicon rods was set to 1.1a. The 3D simulation results demonstrate that the spectral response of the structure closely matches the 2D response (Fig. 13). This consistency indicates that the designed structure not only possesses suitable mechanical stability but also offers reliable optical performance, confirming its practical feasibility.

To accurately evaluate the required power and duration for inducing

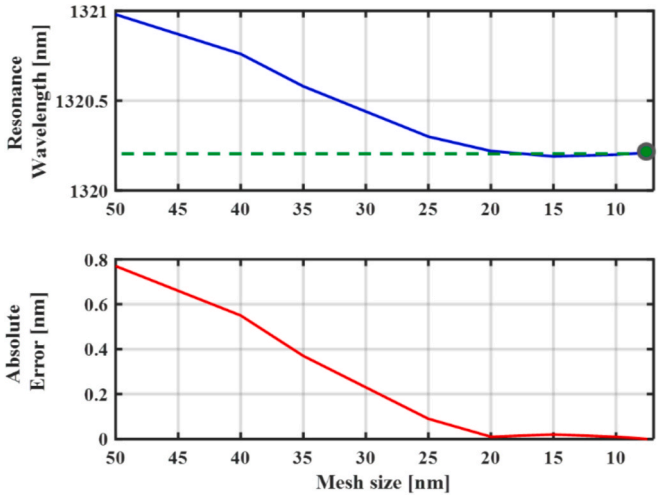

Fig. 12. Mesh size sensitivity analysis for resonance wavelength.

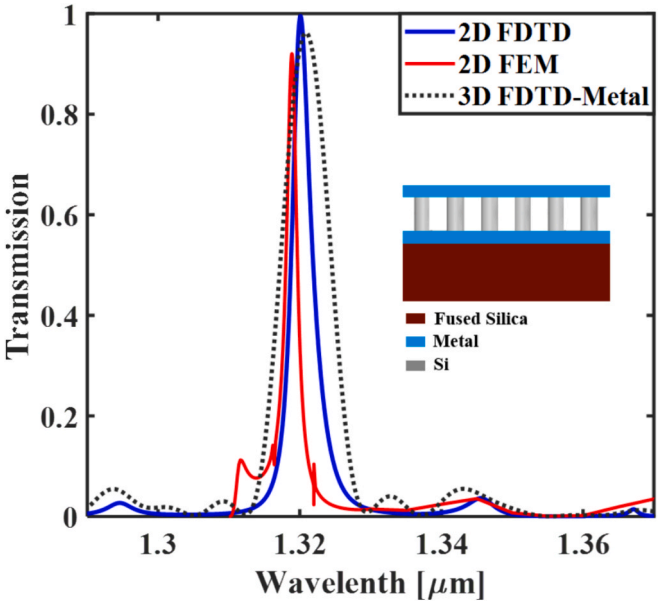

Fig. 13. Comparison of 2D-FEM, 2D-FDTD, and 3D-FDTD simulation results showing consistent spectral responses, confirming design accuracy and practical feasibility.

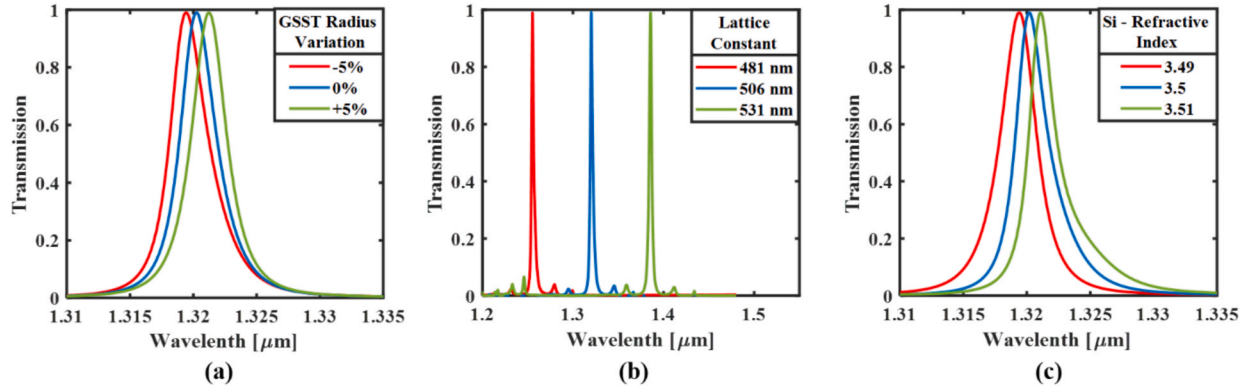

Fig. 11. Tolerance analysis of the photonic crystal synapse structure under fabrication-induced variations: (a) GSST rod radius (±5%), (b) lattice constant (±5%), and (c) silicon refractive index (±0.01). Results confirm stable performance and design robustness.

phase change in the GSST rods, thermal simulations were performed using the finite element method. The results of these simulations are presented in Fig. 14. This thermal modeling enables the examination of the temperature distribution within the structure, as well as the analysis of the GSST crystallinity rate as a function of applied power and time duration. The results indicate that increasing the stimulation power leads to a faster temperature rise, thereby reducing the time needed to achieve the phase transition.

Moreover, the analyses demonstrate that the targeted placement of GSST rods in regions with maximum electric field intensity (as shown in Fig. 6b) significantly enhances phase-switching efficiency and substantially lowers the power required for phase change. This power reduction facilitates the practical implementation of the proposed structure in advanced photonic applications.

Furthermore, based on the theoretical relationships and Eqs. (4)-(8), the increase in electric field intensity in the targeted regions results in a rise in the electromagnetic power loss density (Q_e) within the GSST-PCM [59–63]. These equations, derived from the thermal and optical properties of the PCM, provide an accurate model for analyzing the impact of excitation conditions on the crystallization rate and thermal behavior of the material. The increase in Q_e reflects more efficient conversion of electromagnetic energy into heat within the structure, thereby significantly accelerating the phase-change process. Consequently, for an optical signal with fixed power and energy, the enhancement of the electric field at optimized locations in the structure considerably reduces the time required to reach the desired crystallinity level. This mechanism is a key factor in optimizing energy efficiency and boosting the operational speed of GSST-based phase-change photonics, ensuring device reliability for practical applications.

$$\rho c_p \frac{\partial T}{\partial t} + \rho c_p U.\nabla T = \nabla.(K\nabla T) + Q_e \tag{4}$$

where c_p,ρ and K represent the thermal conductivity, density and specific heat capacity of GSST-PCM, respectively.

$$Q_e = \frac{1}{2} Re(J.E^*) \tag{5}$$

$$J = \sigma E \tag{6}$$

$$\sigma = w\varepsilon_0\varepsilon_2 \tag{7}$$

$$\varepsilon_2 = 2nk \tag{8}$$

where n and k represent the real and imaginary parts of the refractive index of GSST-PCM, respectively, and ε_0 denotes the permittivity of free space.

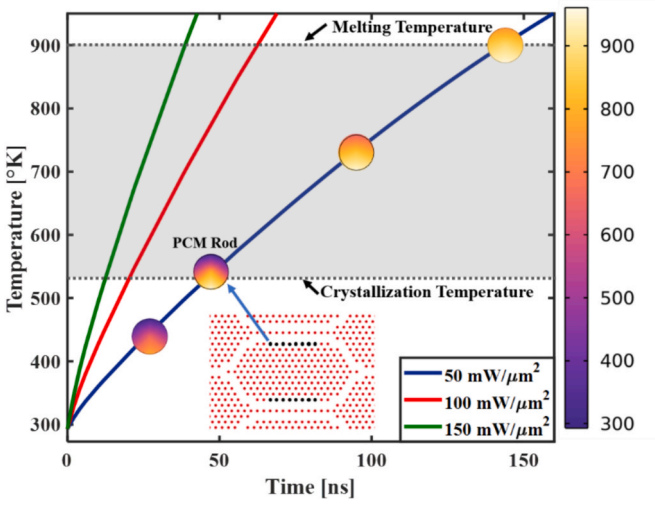

Fig. 14. Thermal simulation of temperature dynamics in GSST-PCM rods for different excitation powers.

Fabrication method

To fabricate the proposed structure, a polymethyl methacrylate (PMMA) layer is spin-coated onto a fused silica substrate. Electron beam lithography (e-beam lithography) is then employed to define the GSST-PCM rod patterns. Subsequently, a germanium-antimony-selenium-telluride film is deposited via atomic layer deposition (ALD) [64,65], precisely filling the etched regions. The remaining polymerized PMMA layer is then removed, and a new PMMA layer is spin-coated onto the fused silica substrate.

In the second lithography step, e-beam lithography is again used to define the silicon (Si) rod patterns. The PMMA resist is selectively etched away, exposing the designated areas for silicon deposition. High-purity silicon rods are then deposited in these regions by chemical vapor deposition (CVD) [66]. After the etching and deposition processes, the remaining PMMA is completely removed.

Conclusion

In this study, an advanced structure for all-optical photonic crystal synapses is presented based on the integration of a Mach-Zehnder interferometer and directional coupler devices. Implementing silicon rods and GSST-PCM rods in photonic crystal structures enables the system to precisely control signal transmission and guidance, thereby enhancing the performance of optical synapses.

The results demonstrate that the proposed structure can achieve precise and low-interference non-volatile optical signal transmission. The transmission at the MZI output exceeded 99 %, which is particularly effective in advanced neural network applications. Additionally, the crystallinity fraction changes of the GSST-PCM rods, induced by applying specific optical signals through directional coupler inputs, significantly affect the signal transmission at the output. The results indicate that in the amorphous and fully crystalline states of the GSST-PCM rods, the signal transmission changes between −0.02 dB and −13.5 dB, highlighting the significant impact of the rods' phase state on the system's performance.

Leveraging the ability to tune transmission and signal guidance across different wavelengths precisely, this photonic crystal-based structure, with dimensions significantly smaller than conventional systems, can serve as an effective tool in the design of optical neural networks and future information processing systems.

Ultimately, this study offers a novel approach for the design and implementation of optical synapses with tunable and controllable transmission, potentially driving transformative advancements in all-optical information processing systems and neuromorphic computing.

Declarations

Ethical approval: We declare that the manuscript entitled "High-performance all-optical photonic crystal synapse based on Mach-Zehnder interferometer and directional coupler utilizing GSST phase-change material" is original, has not been wholly or partly published before, and is not currently being considered for publication elsewhere. In addition, the results are presented honestly without fabrication, falsification, or inappropriate data manipulation. We confirm that the manuscript has been read and approved by all named authors, and that there are no other persons who satisfied the criteria for authorship but are not listed. We further confirm that the order of the authors listed in the manuscript has been approved by all the authors.

CRediT authorship contribution statement

Amir Hossein Abdollahi Nohoji: Writing – original draft,

Validation, Software, Investigation, Conceptualization. **Parviz Keshavarzi:** Writing – review & editing, Supervision. **Mohammad Danaie:** Writing – review & editing, Visualization, Validation, Supervision, Software, Methodology, Conceptualization.

Declaration of competing interest

The authors declare that they have no known competing financial interests or personal relationships that could have appeared to influence the work reported in this paper.

Data availability

Data will be made available on request.

References

[1] Guo X, Xiang J, Zhang Y, Su Y. Integrated neuromorphic photonics: synapses, neurons, and neural networks. Adv Photonics Res 2021;2:2000212.
[2] Rathi N, Chakraborty I, Kosta A, Sengupta A, Ankit A, Panda P, et al. Exploring neuromorphic computing based on spiking neural networks: Algorithms to hardware. ACM Comput Surv 2023;55:1–49.
[3] Yao M, Hu J, Hu T, Xu Y, Zhou Z, Tian Y, Xu B, Li G. Spike-driven transformer v2: Meta spiking neural network architecture inspiring the design of next-generation neuromorphic chips, ArXiv Prepr. ArXiv2404.03663 (2024).
[4] Richter O, Wu C, Whatley AM, Köstinger G, Nielsen C, Qiao N, et al. DYNAP-SE2: a scalable multi-core dynamic neuromorphic asynchronous spiking neural network processor. Neuromorphic Comput Eng 2024;4:14003.
[5] Blankenship BW, Li R, Guo R, Zhao N, Shin J, Yang R, et al. Photothermally activated artificial neuromorphic synapses. Nano Lett 2023;23:9020–5.
[6] Nohoji AHA, Keshavarzi P, Danaie M. A photonic crystal waveguide intersection using phase change material for optical neuromorphic synapses. Opt Mater (amst) 2024;151:115372.
[7] Liu X, Wang D, Chen W, Kang Y, Fang S, Luo Y, et al. Optoelectronic synapses with chemical-electric behaviors in gallium nitride semiconductors for biorealistic neuromorphic functionality. Nat Commun 2024;15:7671.
[8] Zhang T, Fan C, Hu L, Zhuge F, Pan X, Ye Z. A reconfigurable all-optical-controlled synaptic device for neuromorphic computing applications. ACS Nano 2024.
[9] Wang Y, Yin L, Huang W, Li Y, Huang S, Zhu Y, et al. Optoelectronic synaptic devices for neuromorphic computing. Adv Intell Syst 2021;3:2000099.
[10] Gökgöz B, Aydın T, Gül F. Optimizing memristor-based synaptic devices for enhanced energy efficiency and accuracy in neuromorphic machine learning. IEEE Access 2024.
[11] Huo Z, Sun Q, Yu J, Wei Y, Wang Y, Cho JH, et al. Neuromorphic devices assisted by machine learning algorithms. Int J Extrem Manuf 2025.
[12] Luo T, Wong W-F, Goh RSM, Do AT, Chen Z, Li H, et al. Achieving green AI with energy-efficient deep learning using neuromorphic computing. Commun ACM 2023;66:52–7.
[13] Butt MA, Khonina SN, Kazanskiy NL. Recent advances in photonic crystal optical devices: a review. Opt Laser Technol 2021;142:107265.
[14] Sankar Rao DG, Fathima MS, Manjula P, Swarnakar S. Design and optimization of all-optical demultiplexer using photonic crystals for optical computing applications. J Opt Commun 2024;44:s197–202.
[15] Lonergan A, O'Dwyer C. Many facets of photonic crystals: from optics and sensors to energy storage and photocatalysis. Adv Mater Technol 2023;8:2201410.
[16] Arie A. Storing and retrieving multiple images in 3D nonlinear photonic crystals. Light Sci Appl 2021;10:202.
[17] Huang Y, Shi M, Yu A, Xia L. Design of multifunctional all-optical logic gates based on photonic crystal waveguides. Appl Opt 2023;62:774–81.
[18] Liu Y, Qin F, Meng Z-M, Zhou F, Mao Q-H, Li Z-Y. All-optical logic gates based on two-dimensional low-refractive-index nonlinear photonic crystal slabs. Opt Express 2011;19:1945–53.
[19] Jot Singh J, Dhawan D, Gupta N. All-optical photonic crystal logic gates for optical computing: an extensive review. Opt Eng 2020;59:110901.
[20] Laporte F, Katumba A, Dambre J, Bienstman P. Numerical demonstration of neuromorphic computing with photonic crystal cavities. Opt Express 2018;26:7955–64.
[21] Gong Z, Yang F, Wang L, Chen R, Wu J, Grigoropoulos CP, et al. Phase change materials in photonic devices. J Appl Phys 2021;129.
[22] Wei M, Lin X, Xu K, Wu Y, Wang C, Wang Z, et al. Inverse design of compact nonvolatile reconfigurable silicon photonic devices with phase-change materials. Nanophotonics 2024;13:2183–92.
[23] Conrads L, Schüler L, Wirth KG, Wuttig M, Taubner T. Direct programming of confined surface phonon polariton resonators with the plasmonic phase-change material In3SbTe2. Nat Commun 2024;15:3472.
[24] Zhu D, Wang X, Li J, Ye H, Yu Z, Liu Y. Design of nonvolatile and efficient Polarization-Rotating optical switch with phase change material. Opt Laser Technol 2022;151:108065.
[25] Zhang Y, Li Z, Xu S, Xiang Y. Tunable and reconfigurable higher-order topological insulators in photonic crystals with phase change materials. Ann Phys 2022;534:2100293.
[26] Tripathi S, Srivastava V, Sunny RKM. Tuning of resonant mode properties of photonic crystal nanocavities using Ge2Sb2Te5 phase-change material. Indian J Phys 2023;97:3637–42.
[27] Uemura T, Chiba H, Yoda T, Moritake Y, Tanaka Y, Ono M, et al. Nanocavity tuning and formation controlled by the phase change of sub-micron-square GST patterns on Si photonic crystals. Opt Express 2024;32:1802–24.
[28] Wredh S, Wang Y, Yang JKW, Simpson RE. Multi-level optical switching by amorphization in single-and multi-phase change material structures. Adv Opt Mater 2024;12:2301835.
[29] Wang Y, Ning J, Lu L, Bosman M, Simpson RE. A scheme for simulating multi-level phase change photonics materials. npj Comput Mater 2021;7:183.
[30] Chai Z, Fang M, Min X. Composite phase-change materials for photo-thermal conversion and energy storage: a review. Nano Energy 2024;109437.
[31] Bai J, Fei H, Lin H, Wang Y, Zhang M, Liu X, et al. Design of a temperature sensor based on a valley photonic crystal Mach–Zehnder interferometer. Appl Opt 2024;63:4940–5.
[32] Kolli VR, Bahaddur I, Talabattula S. A high sensitive photonic crystal Mach-Zehnder-Interferometer based pressure-sensor. Results Opt 2021;5:100118.
[33] Nohoji AHA, Danaie M. Highly sensitive refractive index sensor based on photonic crystal ring resonators nested in a Mach-Zehnder interferometer. Opt Quantum Electron 2022;54:574.
[34] Saldutti M, Xiong M, Dimopoulos E, Yu Y, Gioannini M, Mørk J. Modal properties of photonic crystal cavities and applications to lasers. Nanomaterials 2021;11:3030.
[35] Phillips CL, Brash AJ, Godsland M, Martin NJ, Foster A, Tomlinson A, et al. Purcell-enhanced single photons at telecom wavelengths from a quantum dot in a photonic crystal cavity. Sci Rep 2024;14:4450.
[36] Chakravarthi S, Yama NS, Abulnaga A, Huang D, Pederson C, Hestroffer K, et al. Hybrid integration of gap photonic crystal cavities with silicon-vacancy centers in diamond by stamp-transfer. Nano Lett 2023;23:3708–15.
[37] Yang J-K, Hwang Y, Oh SS. Evolution of topological edge modes from honeycomb photonic crystals to triangular-lattice photonic crystals. Phys Rev Res 2021;3:L022025.
[38] Danaie M, Kaatuzian H. Improvement of power coupling in a nonlinear photonic crystal directional coupler switch. Photon Nanostruct-Fundam Appl 2011;9:70–81.
[39] Sahoo D, Naik R. GSST phase change materials and its utilization in optoelectronic devices: a review. Mater Res Bull 2022;148:111679.
[40] Khanehzar A, Zamani N, Hatef A. Tunable near-infrared photonic nanostructure: employing the phase transition of GSST for extraordinary optical transmission. J Opt Soc Am B 2024;41:D40–7.
[41] Jiang W. Nonvolatile and ultra-low-loss reconfigurable mode (De) multiplexer/switch using triple-waveguide coupler with Ge2Sb2Se4Te1 phase change material. Sci Rep 2018;8:15946.
[42] Ramchoun H, Ghanou Y, Ettaouil M, Janati Idrissi MA. Multilayer perceptron: Architecture optimization and training; 2016.
[43] Dubey SR, Singh SK, Chaudhuri BB. Activation functions in deep learning: a comprehensive survey and benchmark. Neurocomputing 2022;503:92–108.
[44] Du K-L, Leung C-S, Mow WH, Swamy MNS. Perceptron: Learning, generalization, model selection, fault tolerance, and role in the deep learning era. Mathematics 2022;10:4730.
[45] Auer P, Burgsteiner H, Maass W. A learning rule for very simple universal approximators consisting of a single layer of perceptrons. Neural Netw 2008;21:786–95.
[46] Chakraverty S, Sahoo DM, Mahato NR, Chakraverty S, Sahoo DM, Mahato NR. Delta learning rule and backpropagation rule for multilayer perceptron. Concepts Soft Comput Fuzzy ANN Program 2019:189–95.
[47] Danaie M, Kaatuzian H. Design of a photonic crystal differential phase comparator for a Mach–Zehnderswitch. J Opt 2010;13:15504.
[48] Granpayeh A, Habibiyan H, Parvin P. Photonic crystal directional coupler for all-optical switching, tunable multi/demultiplexing and beam splitting applications. J Mod Opt 2019;66:359–66.
[49] Mohammadi-Pouyan S, Afrouzmehr M, Abbott D. Ultra compact bend-less Mach-Zehnder modulator based on GSST phase change material. Opt Mater Express 2022;12:2982–94.
[50] Mohammadi-Pouyan S, Bahadori-Haghighi S, Rafatmah A, Rahman BMA. Design and analysis of nonvolatile GSST-based modulator utilizing engineered Mach-Zehnder structure with graphene heaters. Opt Laser Technol 2024;169:110088.
[51] Miscuglio M, Meng J, Yesiliurt O, Zhang Y, L.J. Prokopeva, A. Mehrabian, J. Hu, A. V Kildishev, V.J. Sorger, Artificial synapse with mnemonic functionality using GSST-based photonic integrated memory, in: 2020 Int. Appl. Comput. Electromagn. Soc. Symp., 2020: pp. 1–3.
[52] Rashidi A, Hatef A, Entezar SR. Thermally induced tuning of absorption in a Ge2Sb2Te5-based one-dimensional Fibonacci quasicrystal. Opt & Laser Technol 2021;137:106831.
[53] Tolkach NM, Vishnyakov NV, Lazarenko PI, Sherchenkov AA, Sudakova AU, Nazimov DR. Optical switching in multilayer structures based on Ge2Sb2Te5, in. J Phys Conf Ser 2020:12075.
[54] Zhang Y, Chou JB, Li J, Li H, Du Q, Yadav A, et al. others, Broadband transparent optical phase change materials for high-performance nonvolatile photonics. Nat Commun 2019;10:4279.
[55] Gosciniak J. Waveguide-integrated plasmonic photodetectors and activation function units with phase change materials. IEEE Photonics J 2023;16:1–10.
[56] Aly AH, Awasthi SK, Mohamed AM, Al-Dossari M, Matar ZS, Mohaseb MA, et al. 1D reconfigurable bistable photonic device composed of phase change material for detection of reproductive female hormones. Phys Scr 2021;96:125533.

[57] Pourmand M, Choudhury PK. Programmable phase-change medium-assisted hyperbolic metamaterial as a dual-band nearly perfect absorber. JOSA B 2022;39:1222–8.
[58] Rashidi S, Rashidi A, Entezar SR. Tunable NIR absorption in a Ge2Sb2Te5-based 1D asymmetric nonlinear hybrid nanostructure. Opt & Laser Technol 2023;157:108664.
[59] Saemathong J, Pannucharoenwong N, Mongko V, Vongpradubchai S, Rattanadecho P. Analyzing two laser thermal energy calculation equations: a comparison of beer-lambert's law and light transport equation. Eng Sci 2023;24:912.
[60] Savini A, Turowski J. Electromagnetic fields in electrical engineering. Springer Science & Business Media; 2012.
[61] Consoli F, Tikhonchuk VT, Bardon M, Bradford P, Carroll DC, Cikhardt J, et al. Laser produced electromagnetic pulses: generation, detection and mitigation. High Power Laser Sci Eng 2020;8:e22.
[62] Bounouar A, Gueraoui K, Taibi M, Lahlou A, Driouich M, Sammouda M, et al. Numerical and mathematical modeling of unsteady heat transfer within a spherical cavity: applications laser in medicine. Contemp Eng Sci 2016;9:1183–99.
[63] Balanis CA. Advanced engineering electromagnetics. John Wiley & Sons; 2012.
[64] Eom T, Choi S, Choi BJ, Lee MH, Gwon T, Rha SH, et al. Conformal formation of (GeTe2)(1–x)(Sb2Te3) x layers by atomic layer deposition for nanoscale phase change memories. Chem Mater 2012;24:2099–110.
[65] Guo P, Sarangan AM, Agha I. A review of germanium-antimony-telluride phase change materials for non-volatile memories and optical modulators. Appl Sci 2019;9:530.
[66] Fujisaki Y, Sasago Y, Kobayashi T. Amorphous thin GeSbTe phase-change films prepared by radical-assisted metal-organic chemical vapor deposition. Thin Solid Films 2015;583:55–9.